HHS Public Access

Author manuscript

Magn Reson Med. Author manuscript; available in PMC 2016 May 23.

Published in final edited form as:

Magn Reson Med. 2009 February ; 61(2): 399–408. doi:10.1002/mrm.21863.

PARACEST MRI With Improved Temporal Resolution

Guanshu Liu, **M. Meser Ali**, **Byunghee Yoo**, **Mark A. Griswold**, **Jean A. Tkach**, and **Mark D. Pagel***

Departments of Biomedical Engineering and Radiology, Case Western Reserve University, Cleveland, Ohio

Abstract

PARAmagnetic Chemical Exchange Saturation Transfer (PARACEST) is a novel contrast mechanism for MRI. A PARACEST MRI methodology with high temporal resolution is highly desired for in vivo MRI applications of molecular imaging. To address this need, a strategy has been developed that includes a long selective saturation period before each repetition of a Rapid Acquisition with Relaxation Enhancement (RARE) pulse sequence. This strategy is suitable for the application of PARACEST contrast agents to environments with long T_1 relaxation times. An alternative strategy uses short selective saturation periods before the acquisition of each *k*-space trajectory to maintain steady state conditions, which can be implemented with a Fast Low Angle Shot (FLASH) pulse sequence. These short saturation periods lengthen the total scan time as compared to the first approach but compensate for the loss in PARACEST contrast related to T_1 relaxation. Both approaches have been demonstrated in vitro and in vivo with significantly improved temporal resolutions as compared to a conventional gradient-echo PARACEST method without sacrificing CNR efficiency. These demonstrations also adopted a strategy for measuring the PARACEST effect that only requires selective saturation at a single MR frequency, which further improves temporal resolution for PARACEST detection.

Keywords

MRI; PARACEST contrast agent; temporal resolution

Chemical Exchange Saturation Transfer (CEST) is a novel MRI contrast mechanism that is an attractive alternative to T_1 and T_2 contrast mechanisms (1), particularly at high magnetic fields (2). CEST agents possess a hydrogen proton with a moderate to slow exchange rate with water. Selective saturation of the MR frequency of this proton, followed by exchange with solvent water, reduces the MR signal of the water. PARACEST (PARAmagnetic CEST) agents include a paramagnetic lanthanide ion that shifts the MR frequencies of the exchangeable proton to unique values to facilitate selective detection (3,4). Endogenous MR contrast may be continually monitored in the presence of PARACEST agents by neglecting to saturate the MR frequency of the exchangeable proton (and assuming that the T_1 relaxation of the PARACEST agent is negligible). Selectively detectable PARACEST agents have been designed to respond to enzymes (5), metabolites (6,7), metal ions (8), tissue pH

*Correspondence to: Mark D. Pagel, Departments of Biomedical Engineering and Radiology, Case Western Reserve University, 10900 Euclid Avenue, Cleveland, Ohio 44106-7207. ; Email: mpagel@case.edu

(3,9), and temperature (10). Therefore, responsive PARACEST agents may have particular advantages for molecular imaging applications.

In vivo applications of “off-resonance” PARACEST MRI have not been established due in part to the formidable challenges of low sensitivity and poor temporal resolution. In general, the PARACEST effect is measured through asymmetric analysis of coherent magnetization M_S after selective saturation at Δω (frequency with respect to water resonance frequency) and −Δω (Eq. [1]).

$$\%\mathrm{PARACEST}\,(\Delta\omega) = 1 - \mathrm{M_s}(\Delta\omega)/\mathrm{M_s}(-\Delta\omega) \quad [1]$$

Therefore, two image acquisitions at saturation frequencies of Δω and −Δω are required for a quantitative PARACEST study. In practice, a long saturation scheme is also required in addition to the imaging scheme for full saturation transfer between two proton pools before each *k*-space acquisition (3). As a example, with the use of a saturation pulse of approximately 2 s, the total scan time for a standard quantitative PARACEST study can be as long as 10 min, which includes the acquisition of two MR images (M_S(Δω) and M_S(−Δω)) with 128 phase encoding steps. It is impractical to apply PARACEST agents to a dynamic in vivo study with such poor temporal resolution. Therefore, the development of PARACEST MRI methods with improved temporal resolution is highly desirable for in vivo applications of PARACEST agents.

Some biomedical applications require the monitoring of biological processes with a temporal resolution that is much faster than 10 min. For example, the accumulation of small molecule MRI contrast agents in tumors and normal tissues can often occur within the first 10 min after the agent is injected into the vasculature, followed by a washout of the agent from the tissue during the subsequent 10–30 min (11). Although temporal resolutions approaching 1 s can most accurately determine the rates of these pharmacokinetic processes (12), a temporal resolution on the order of 10–90 s can be sufficient to estimate these rates (13,14). Therefore, PARACEST MRI methods with a temporal resolution of approximately 10–90 s could be used for Dynamic Contrast Enhanced (DCE) MRI studies of pharmacokinetics processes.

As we describe here, the temporal resolution of PARACEST studies may be greatly improved by using faster MRI methods, such as a multiple-echo acquisition scheme (Fig. 1A). The temporal resolution may also be improved by using MRI methods with faster selective saturation periods, such as an interleaved repetitive short saturation-acquisition scheme (Fig. 1B). In this report, both methods are compared with each other and with a standard PARACEST MRI method to assess the impact of improved temporal resolution on PARACEST contrast, contrast-to-noise (CNR), and CNR efficiency. Furthermore, both methods are applied to in vivo MRI studies to investigate the ability to detect PARACEST agents within in vivo tissues with fast temporal resolution.

THEORY

PARACEST can be described by a two-site exchange model for most cases (3,15) or can be simplified to be a two-site exchange model in more complicated situations (16). A two-site exchange PARACEST system consists of a bulk free water proton pool (W) and a small labile proton pool on a contrast agent (CA) that is water-exchangeable. The longitudinal magnetization of bulk water can be described by a simplified Bloch-McConnell equation (17) with assumption of instantaneous and complete saturation of pool CA and no direct saturation of the pool W (Eq. [2]).

$$\frac{dM^W}{dt}=M_0^W/T_{1W}-M^W(1/T_{1W}+1/\tau_W) \quad [2]$$

M^W: MRI signal or the magnetization of pool W

M_0^W: the equilibrium magnetization of pool W

T_{1W}: longitudinal relaxation time of pool W in the presence of saturation

τ_W: the proton residence life times in pool W

At thermal equilibrium, the exchange rates between the two pools have a mass balance (Eq. [3]).

$$M_0^W/M_0^{CA}=\tau_W/\tau_{CA} \quad [3a]$$

or

$$\tau_W=\tau_{CA}\frac{[\text{proton}]_W}{[\text{proton}]_{CA}}=\tau_{CA}\frac{2[H_2O]}{n[CA]} \quad [3b]$$

where τ_{CA} is the proton residence life times in pool CA.

In Eq. [3b], n is the number of exchangeable protons on the PARACEST agent and [H_2O] and [CA] are the concentrations of water and the PARACEST agent, respectively.

The Bloch-McConnell equation can be solved using numerical (4,16) or analytical (18) methods. A steady state analytical method (Eq. [4]) is most often used to provide contrast quantification while a transient analytical solution can provide more useful information for the exchange rate estimation (3,4) as well as for method optimization (Eq. [5]).

$$\frac{M_S}{M_0}=\frac{\tau_W}{T_{1W}+\tau_W} \quad [4a]$$

or

$$\frac{M_S}{M_0}=1/\left(1+\frac{nT_{1W}[CA]}{2\tau_{CA}[H_2O]}\right) \quad [4b]$$

$$\frac{M_S(\tau_S)}{M_0}=\frac{\tau_{1W}}{T_{1W}}+\frac{\tau_{1W}}{\tau_W}e^{(-\tau_S/\tau_{1W})} \quad [5]$$

In Equations [4] and [5], M_S and M_0 represent the coherent magnetization of the pool W with or without saturation, respectively. Also, τ_{1W} represents the effective residence lifetime of pool W (Eq. [6]).

$$\frac{1}{\tau_{1W}}=\frac{1}{T_{1W}}+\frac{1}{\tau_W} \quad [6]$$

As is evident from Equation [5], the attenuation of the MR signal of the water pool depends on the length of the RF pulse (τ_S, time of saturation). To maximize the PARACEST contrast, one should maximize the time of saturation, as is typically done in PARACEST experiments which use a very long τ_S (> 2 s) to ensure the establishment of the steady state of M_S (Eq. [4]), especially when T_1 is also long (3,15). Upon the removal of the saturation RF pulse, the M_S of pool W relaxes to the thermal equilibrium state (M_0) at a rate equivalent to its native longitudinal relaxation rate ($R_{1W} = 1/T_{1W}$) (18). The recovery of magnetization after saturation causes the loss of PARACEST contrast. Therefore, the ideal PARACEST MRI acquisition would record the signal immediately after the steady state of CEST is established, which is the typical scheme used for a NMR PARACEST study.

This formalism can be extended for MRI studies with an effective echo time (TE^{eff}, the time between excitation pulse and the center of echo; Eq. [7]). This full temporal dependence of M_S can be modeled with numerical methods. Two boundary conditions can provide an intuitive understanding of this temporal dependence. When $TE^{eff} \ll T_{1w}$, the PARACEST contrast is maximized when $\tau_S \gg \tau_{1W}$. When $TE^{eff} \gg T_{1W}$, the PARACEST contrast approaches zero. Therefore, a short echo time and a long saturation time provide ideal PARACEST contrast.

$$\frac{M_S\left(\tau_S,\, TE^{eff}\right)}{M_0}=1-\frac{\tau_{1W}}{\tau_W}\cdot e^{(-TE^{eff}/T_{1W})}\cdot\left(1-e^{(-\tau_S/\tau_{1W})}\right) \quad [7]$$

As indicated in Equation [7], endogenous T_2 relaxation does not affect the PARACEST measurement. Although T_2 relaxation can affect the *absolute* amplitudes of the MR signal with and without transferred saturation, T_2 relaxation cannot affect the *relative* amplitudes of the MR signal that are used to measure PARACEST. After the transfer of saturation, slice selection and phase encoding, the total net magnetization consists of coherent magnetization in the transverse plane and incoherent magnetization that “points” in all directions about the origin. The MR spins of the coherent and incoherent magnetizations can “share” spin–spin interactions that lead to T_2 relaxation, so that the coherent magnetizations with or without

transferred saturation have the same T_2 relaxation times. At TE > 0, the same T_2 relaxation rates will decrease the *absolute* amplitudes of the coherent magnetizations with or without transferred saturation, but their *relative* amplitudes will remain the same.

Conversely, endogenous or static T_1 relaxation affects the PARACEST measurement, as indicated by the first exponential term in Equation [7]. After transferred saturation, slice selection and phase encoding, the sum of the T_1 relaxation of the coherent and incoherent magnetizations must equal the sum of the T_1 relaxation of the coherent magnetization without saturation, because the number of spin–lattice interactions that stimulate magnetization to return to equilibrium are the same with or without transferred saturation. In effect, the coherent magnetization "competes" with the incoherent magnetization for these spin–lattice interactions, which causes the T_1 relaxation rate of the coherent magnetization after transferred saturation to be slower than that the T_1 relaxation rate of the coherent magnetization with no saturation. This decreases the *relative* difference in amplitudes of the MR signal with and without saturation, which decreases the measurement of PARACEST.

The consequences of this theoretical analysis are best assessed by comparing Equation [7] under practical conditions with the theoretical steady-state PARACEST effects calculated with Equation [4b]. A typical PARACEST agent, 20 mM Eu(III)DOTAM-Gly (**Eu(1)**), has a chemical exchange rate of 3.3 KHz at 298 K (19). Typical tissues in high magnetic field strengths have relatively short, moderate and long T_1 relaxation, or a T_{1W} of 1, 2 or 3 s, respectively. A saturation pulse train that is commonly available on preclinical MRI scanners consists of 1000 Gaussian pulses with a pulse length of 2.25 ms and inter-pulse delay of 10 μs, or a τ_S of 2.26 s. To improve the temporal resolution under the same saturation conditions, an acquisition scheme with a longer effective echo time may be used. For example, a typical effective TE (TE^{eff}, or the time for half of the echo train duration) for a Rapid Acquisition with Relaxation Enhancement (RARE) spin-echo acquisition scheme may be as long as 320 ms. These conditions generate simulated PARACEST effects that are very close to the maximum values of simulated steady state CEST contrast for each value of T_{1w} (Fig. 2; Table 1). For comparison, an analysis of a train of 1500 Gaussian pulses during a τ_S of 3.4 s shows only very minor additional improvement in CEST contrast for each T_{1W} value, which demonstrates that a τ_S of 2.26 s had effectively reached the steady state. The loss of PARACEST contrast after the end of τ_S is strongly dependent on T_{1W} (Fig. 3; Table 1). For a T_{1W} of 3 s, the PARACEST contrast suffers only a relatively minor loss of 12.8% at the end of a TE^{eff} of 320 ms. However, for a T_{1W} of 1 s, the longitudinal relaxation is too fast to avoid a more substantial 27.8% loss of PARACEST contrast.

To improve the temporal resolution while retaining a short echo time, a shorter saturation time may be used. For example, a Fast Low Angle Shot (FLASH) sequence with Gaussian saturation pulses that fill TR times of 100, 200 or 300 ms can be evaluated with a T_{1W} of 1, 2, or 3 s and the same properties of 20 mM **Eu(1)** as listed above. These conditions quickly achieve a steady state of saturation of pool W within 30 repetitions and effectively maintain the steady state PARACEST by compensating for relaxation loss of PARACEST contrast before each acquisition (Fig. 3). Similar to the simulations of the RARE method, these simulations of the FLASH method showed a strong dependence of PARACEST contrast on the T_{1W} of the sample (Table 2). The PARACEST effects were relatively independent of the

saturation time of the steady-state saturation scheme. These simulations also showed that, for each T_{1W}, the FLASH method with TR of 100, 200, and 300 ms generated more PARACEST contrast than the RARE method with TE^{eff} of 320 ms.

METHODS

Chemicals

Eu(III)DOTAM-Gly (**Eu(1)**) and Tm(III)DOTAM-Gly (**Tm(1)**) (Fig. 4) were synthesized according to published procedures (3,20) and used as model PARACEST agents for phantom studies. **Tm(1)** was also used for tumor PARACEST DCE MRI studies. Eu(III)DOTA-OBS2Gly2-COOH (Eu(III)1,7-Bis (2-(methylene benzyloxy ether)-acetic acid) acetamide-4,10-bis (acetamidoacetic acid)-1,4,7,10-tetraazacyclododecane; **Eu(2)**; Fig. 5) was synthesized and characterized according to published procedures (21) and used for in vivo liver studies. These published procedures have also demonstrated that **Eu(1)** and **Eu(2)** possess very similar T_1 relaxation and PARACEST properties, even though **Eu(2)** has a threefold slower exchange rate than **Eu(1)**. The labile protons that generate PARACEST signals are bound-water protons for **Eu(1)** and **Eu(2)**, and amide proton for **Tm(1)**, respectively. The PARACEST saturation frequencies of **Eu(1)**, **Eu(2)** and **Tm(1)** were confirmed to be +50 ppm, +54 ppm and −51 ppm, respectively, by means of NMR spectroscopy of samples dissolved in H_2O with 10% D_2O.

The concentrations of PARACEST MRI phantoms were 20 mM for **Eu(1)** and 20 mM for **Tm(1)**. The concentrations of phantoms used to measure T_1 relaxivities were 0, 12.5, 25, and 50 mM for **Eu(1)** and 2.5, 5, 10, and 20 mM for **Tm(1)**. All phantoms used phosphate-buffered saline to maintain a pH of 7.4. All phantom studies were conducted at 37 ± 0.2°C using a temperature probe and an air heater (SA Instruments, Inc.).

In vivo Animal Studies

All in vivo studies were conducted according to approved procedures of the Institutional Animal Care and Use Committee of Case Western Reserve University. A mouse model with a subcutaneous tumor of MCF-7 human mammary carcinoma was prepared by injecting 1.5 M MCF-7 tumor cells in 0.5 mL of 50% Matrigel into the right lower flank of a 6-week-old female athymic NCR nu/nu mouse. An 18-week-old Balb/C mouse was used to study PARACEST MRI in liver tissues. To prepare for the MRI exam, each mouse was anesthetized with 1.5–2.0% isoflurane delivered in 2 L/min oxygen gas ventilation. A 26 g dental catheter was inserted in the tail vein to facilitate the administration of 3.2 mmol/kg **Eu(2)** or 4.0 mmol/kg **Tm(1)** in 100 μL that was infused over 30 s. The mouse was then secured to a customized MRI-compatible cradle, probes for monitoring rectal temperature and respiration were connected to the mouse, and core body temperature was regulated at 37 ± 0.2°C using an automated feedback loop between the temperature probe and an air heater (SA Instruments, Inc). At the conclusion of the MRI scan, the mouse was removed from the MRI magnet and cradle, and killed with CO_2 asphyxiation before recovery from anesthesia.

Optimization of MRI Acquisition Procedures

To optimize various acquisition procedures for PARACEST, several different MRI methods were tested. To simplify the analysis, single slice acquisitions were used in all studies. A Gradient Echo MRI method with a single echo was prepended with a selective saturation period to create a presat-GRE pulse sequence (TR = 2.267 s, TE = 2.006 ms). This selective saturation period consisted of a train of 1000 Gaussian RF pulses (power = 20 μT, duration = 2.25 ms, bandwidth = 1218 Hz, inter-pulse delay = 10 μs) followed by a 258 μs spoiling gradient to remove residual transverse magnetization at the end of each τ_S period. To quantify the PARACEST effect according to Equation [1], images were acquired with selective saturation applied at the on-resonance frequency ($\Delta\omega$), and the opposite saturation frequency ($-\Delta\omega$) with respect to the water resonance offset. The presat-GRE method used a NMR-like saturation and acquisition scheme, and, therefore, could be used as standard CEST method for quantitative comparison.

To investigate the strategy of multiple-echo acquisition, a presat-RARE MRI pulse sequence was developed that consisted of a conventional RARE method (22,23) (RARE factor = 1, 4, 8, 16, 32 or 64, TR = 2.279–2.761 s depending on the RARE factor, TE = 7.659 ms) that was prepended with the same selective saturation period as the presat-GRE method (Fig. 1A). To investigate the strategy of short steady-state saturation, a presat-FLASH MRI pulse sequence was developed from a conventional FLASH method (24) (TR = 100 ms, 200 ms, or 300 ms, flip angle = 39°, 41°, 43°, TE = 2.006 ms) that was prepended with selective saturation. This saturation consisted of 41, 85, or 129 Gaussian RF pulses that filled the given TR (Fig. 1B), with the same pulse duration and power as the presat-GRE method. The second of two successive presat-FLASH images were used for the analyses to ensure steady-state saturation. Only the time for acquiring the second image was used to determine CNR efficiencies of this method to relate the in vitro studies to in vivo studies with continuous image acquisitions. All in vitro PARACEST MRI measurements used a 128 × 128 matrix size, one average, and an excitation bandwidth of 101,010 Hz. MRI studies were performed with a 9.4T Bruker Biospec animal MRI scanner (Bruker Biopsin Co. Billerica, MA) equipped with a 35-mm birdcage RF coil.

The Contrast-to-Noise (CNR) Efficiency was used to quantitatively compare different PARACEST MRI methods in addition to the PARACEST contrast and temporal resolutions. The image contrast was obtained by subtracting the precontrast image from the postcontrast image. The contrast was quantified as the mean of the ROI in the contrast image and the noise was estimated by the standard deviation (δ) of the air noise area and multiplied by $\sqrt{2}$ (25). The CNR efficiency was calculated as the ratio of contrast to noise ratio and the square root of the acquisition time for MR images acquired with both saturation frequencies (t_{total}) according to Equation [8].

$$\text{CNR Efficiency} = \text{contrast} / (\sqrt{2} \cdot \delta \cdot \sqrt{t_{total}}) \quad [8]$$

In vivo DCE MRI studies of tumor tissue were conducted by using a presat-RARE method with a RARE factor of 16 (TR = 5000 ms, 256 × 256 matrix size, single average). A continuous series of PARACEST MR images were acquired with selective saturation applied

at −51 ppm for **Tm(1)**. The saturation pulses and other MR parameters were the same as the in vitro presat-RARE method as described above. The total acquisition time for one presat-RARE image was 80 s.

In vivo DCE MRI studies of liver tissue were conducted by using a presat-FLASH method with a TR of 300 ms (128 × 128 matrix size, two averages). A continuous series of PARACEST MR images were acquired with selective saturation applied at +54 ppm for **Eu(2)**. The saturation pulses and other MR parameters were same as the in vitro presat-FLASH method as described above. The total acquisition time for one presat-FLASH image was 76.8 s.

For all in vivo studies, the PARACEST agent was injected immediately after the third PARACEST MR image was acquired. Unlike previously published PARACEST MRI studies, selective saturation was not applied at −54 ppm or +50 ppm to measure $M_S(-\Delta\omega)$ for quantifying each PARACEST effect. Instead, the PARACEST contrast was quantified within each image by substituting the average M_S during the first 3 images for $M_S(-\Delta\omega)$ in Equation [1]. This procedure avoided an interruption in continuous selective saturation at a single MR frequency.

A spin-echo MRI experiment was used to determine T_1 relaxation times of phantoms of **Eu(1)** and **Tm(1)** (TR = 0.2, 0.5, 1, 1.5, 2, 3, 4.5, 6, 8, 12, 15, and 20 s, TE = 11.2 ms, flip angle 90°, one average). A similar MRI experiment was used to determine T_1 relaxation times of an in vivo flank tumor and liver tissue (TR = 0.1, 0.3, 0.6, 1, 1.5, 2.25, 3.5, 5, 7.5, and 10 s, TE = 11.2 ms, flip angle = 90°, one average). To calculate T_1 relaxation times, T_1-weighted MR images were processed with PARAVISION (Bruker Bio-spin Inc) or the MRI analysis calculator package of ImageJ (NIH) (26). The PARACEST MR images were analyzed with ImageJ and MS Excel (Microsoft, Seattle, WA).

RESULTS

Phantom Studies

Quantitative studies were conducted with phantoms containing 20 mM of **Eu(1)** or **Tm(1).** **Eu(1)** had a very low T_1 relaxivity ($r1 = 0.0018\ mM^{-1}\ s^{-1}$) and the addition of 20 mM of this agent to phosphate buffered saline (PBS) caused a nearly negligible change in T_1 relaxation time from 5.0 s to 4.2 s. Therefore, **Eu(1)** represented a model PARACEST agent with slow T_1 relaxation for the study of presat-RARE and presat-FLASH methods. **Tm(1)** had a relative high T_1 relaxivity ($r1 = 0.074\ mM^{-1}s^{-1}$). The addition of 20 mM of **Tm(1)** to PBS caused the T_1 relaxation time to be drastically shortened from 5.0 s to 0.58 s. Therefore, this sample of **Tm(1)** was selected as an example of a PARACEST agent with relatively fast T_1 relaxation for the study of presat-RARE and presat-FLASH methods.

The presat-RARE method showed improvements in temporal resolution relative to the presat-GRE method that scaled with the RARE factor, reaching a 52.8-fold improvement in temporal resolution for a RARE factor of 64 (Table 3). The detection of PARACEST with the presat-RARE method decreased with an increasing RARE factor for both **Eu(1)** and **Tm(1)**. This decrease was relatively minor for **Eu(1)** with slow T_1 relaxation, with a loss in

PARACEST detection that was no greater than 9.47% with a RARE factor of 64 relative to a presat-GRE method. The comparison of the same methods for **Tm(1)** with fast T_1 relaxation resulted in up to a 38.05% loss in PARACEST detection with a RARE factor of 64 relative to presat-GRE. These results agreed with the trends observed from the simulations of presat-GRE and presat-RARE methods with T_{1W} of 3 s and 1 s. Furthermore, the presat-RARE method retained similar CNR efficiencies relative to the presat-GRE method for **Eu(1)**, especially with RARE factors of 4, 8 and 16, while the presat-RARE method showed a continual decrease in CNR efficiencies with an increasing RARE factor relative to the presat-GRE method for **Tm(1)**.

The presat-FLASH method improved the temporal resolution relative to the presat-GRE method by factors of 7.6, 11.3, and 22.7 for a TR of 300, 200, and 100 ms, respectively. The detection of PARACEST with the presat-FLASH method showed a decrease with a decreasing saturation time for both **Eu(1)** and **Tm(1)**, which differed from the simulations. Furthermore, the presat-FLASH method showed a 21.22–26.57% loss in PARACEST detection for **Eu(1)**, and a 10.83–28.52% loss in PARACEST detection for **Tm(1)**, relative to presat-GRE, which also differed from simulations. The CNR efficiency of the presat-FLASH method was more than an order of magnitude lower than the CNR efficiency of the presat-GRE method for **Eu(1)**, while the CNR efficiencies were comparable for the presat-FLASH and presat-GRE methods for **Tm(1)**, especially for a presat-FLASH method with a TR of 300 ms.

In vivo Studies

Both presat-RARE and presat-FLASH methods were used to perform in vivo PARACEST MRI studies, particularly to investigate the applicability of PARACEST agents for DCE MRI studies. The presat-RARE method was successfully applied to a PARACEST DCE MRI study of a subcutaneous flank tumor using **Tm(1)**. The endogenous T_1 relaxation time of the flank tumor was measured to be 3.08 s, which was sufficiently long for a presat-RARE method with a RARE factor of 16 while still retaining good PARACEST detection (Fig. 5). To achieve a 95% and 99% probability that the contrast before and after injection of the agent was different, the CNR must reach $2\sqrt{2}$ and $3\sqrt{2}$, respectively (25). The 99% CNR probability threshold was achieved 21 min after injection of the agent, when a 1.97% change in MR signal was observed. Preliminary studies with an injection concentration of 0.2 mmol/kg of **Tm(1)** did not produce detectable PARACEST (data not shown), which further validated that PARACEST is caused by introduction of a high concentration of **Tm(1)** and not by the injection procedure.

The presat-FLASH method was applied to a DCE MRI study of liver tissue (Fig. 6), which had a relatively shorter T_1 relaxation time of 1.27 s. This in vivo study used **Eu(2)**, a derivative of **Eu(1)** that included two hydrophobic o-benzyl functionalities (oBzl ligands) to improve the retention time in liver tissue. Furthermore, the amounts of the injected agent was 20–40 times higher than used in most preclinical and clinical studies (typically 0.1–0.2 mmol/kg), which also improved the tissue accumulation and lengthened the retention time of each agent. The 95% CNR probability threshold was achieved 14.08 min after injection of the agent, when a 7.04% change in MR signal was observed, and the 99% CNR probability

threshold was achieved 47.36 min after injection of the agent, when a 22.09% change in MR signal was observed.

Each postinjection image was compared with the average of the preinjection images to quantify PARACEST contrast, which required selective saturation at only one MR frequency. Using the average of the preinjection images was particularly important for minimizing the effect of motion artifacts during in vivo liver MRI studies. The temporal resolutions were 80 s per presat-RARE image and 76.8 s per presat-FLASH image, which greatly aided the visualization of contrast agent uptake.

DISCUSSION

The T_1 relaxation times of the PARACEST agent and the sample dictate the selection of the fast method that will produce the greatest PARACEST effect, CNR, or CNR efficiency. A presat-RARE method provided better PARACEST contrast than a presat-FLASH method when the T_1 relaxivity of the agent was low and the endogenous T_1 relaxation time of the water pool was long. Although the CNRs of the presat-RARE methods were lower than the CNR of the presat-GRE method for the **Eu(1)** phantom study, a RARE factor up to 64 still provided a PARACEST CNR that was greater than the 95% probability threshold. In this study, the CNR efficiency was greatest when a RARE factor of 16 was used. In addition, the signal amplitude of the sample was lower for the presat-FLASH method for **Eu(1)**, which resulted in a lower CNR and CNR efficiency with this method for this sample.

A presat-FLASH method with a TR of 300 ms provided better CNR and CNR efficiency than a presat-RARE method when the T_1 relaxation caused by the agent was high and/or the endogenous T_1 relaxation time of the water pool was short. For the **Tm(1)** phantom study, only the presat-FLASH method with a TR of 300 ms generated a CNR that was above the 95% probability threshold for assigning the contrast to the presence of the PARACEST agent, and generated a CNR efficiency that was comparable to the CNR efficiency of presat-GRE (25). The signal amplitude of the sample was lower for the presat-RARE method, which contributed to a lower CNR and CNR efficiency with this method. The detected PARACEST contrast was strongly dependent on the TR time or RARE factor for this sample that had rapid T_1 relaxation.

These analyses clearly show that the exact PARACEST MRI pulse method used has a strong influence on the CNR and CNR efficiency, and that one must take into account the full CNR of the image, not simply the contrast level. For example, a presat-RARE with a RARE factor of 16 detected a 34.48% PARACEST effect from **Eu(1)**, while presat-FLASH using a TR of 300 ms detected a 28.54% PARACEST effect. These relatively similar contrast levels may lead to the conclusion that these two experiments produced comparable results. Yet the statistical significance of MRI contrast is a function of CNR and CNR efficiency and not just the contrast level. This presat-RARE experiment yielded a CNR of 11.12 and CNR efficiency of 1.80, which was much greater than the 1.61 CNR and 0.18 CNR efficiency of the presat-FLASH experiment, leading to the proper conclusion that the presat-RARE experiment outperformed the presat-FLASH experiment for this in vitro sample. Therefore, reports of PARACEST MRI should include the CNR and/or CNR efficiency, and a

comparison to the 95% or 99% CNR probability levels (or other CNR levels of statistical significance as needed), along with the pulse sequence and parameters. These reports of CNRs and/or CNR efficiencies will improve on the current practice of considering a relatively arbitrary 5% contrast threshold as sufficiently significant for PARACEST MRI studies (7,27).

The simulations and experimental results were in agreement for the presat-RARE method, but showed differences for the presat-FLASH method. The simulations predicted that a presat-FLASH method that had reached steady-state conditions would detect the same amount of PARACEST contrast as the presat-GRE method, but the experimental results showed a lower detection of PARACEST with presat-FLASH. The simulations predicted that PARACEST detection would be independent of TR, but the experimental results showed that PARACEST detection was dependent on TR. These differences may indicate that the assumption of instantaneous and complete saturation of the contrast agent that was used in the theory of the simulations may not be appropriate for the presat-FLASH method, or that the selective saturation method used in this study does not meet this assumption. Additional studies are warranted to understand these differences between simulations and experiments for the presat-FLASH method.

As with other RARE methods (28), the spatial resolution in a presat-RARE image is also compromised as a consequence of the T_2 relaxation over the course of the echo train, especially when the T_2 relaxation time is relatively short. A RARE factor of 16 was used for in vivo studies in this report to maintain good spatial resolution for in vivo presat-RARE MRI acquisitions. T_2 relaxation does not affect the quantification of PARACEST as described in the Theory section.

The improved temporal resolutions of presat-RARE and presat-FLASH provided the opportunity to perform practical in vivo PARACEST DCE MRI studies. Presat-RARE and presat-FLASH methods were used for the in vivo detection of a contrast agent in tissue with a long T_{1W} and short T_{1W}, respectively. However, the choice of a fast MRI acquisition method should be based on the T_{1W} relaxation time of the tissue when it contains the contrast agent, because the contrast agent may significantly contribute to the T_{1W} relaxation. The amount of accumulation of contrast agent in the tissue can be used to estimate the T_{1W} relaxation time of the tissue with agent. When the amount of accumulation of the agent cannot be anticipated before an in vivo study, then the best recourse is to select the choice of the fast MRI acquisition method on the endogenous T_{1W} of the tissue for a preliminary test. This rationale is exemplified by the initial study of **Tm(1)** accumulation in tumor tissue as detected with a presat-RARE sequence (Fig. 5), in which the level of accumulation of **Tm(1)** in the tumor tissue was not previously known. Yet additional studies of **Tm(1)** accumulation in tumor tissue may show that the presat-FLASH sequence can provide improved PARACEST detection relative to this initial study.

In both in vivo studies, the image contrast before and after injection of the agent reached a level of 99% probability that the dynamic change in contrast was real. This dynamic change in image contrast was attributed to the accumulation of the PARACEST agent within the in vivo tissues, because this accumulation was assumed to be the only dynamic change in each

mouse after injection of the agent. In addition to creating a PARACEST effect, the contrast agent may also cause dynamic changes in T2 relaxation, bulk magnetic susceptibility effects, line broadening due to chemical exchange, and changes to the magnetization transfer effect. Each of these effects are estimated to cause minor changes in image contrast that are less than the detected contrast changes for these PARACEST agents used for in vivo studies. However, additional studies are warranted before the changes in MR signal after selective saturation can be conclusively ascribed to the PARACEST effect. In particular, all of these effects may be evaluated with a MR CEST Spectroscopic Image, which consists of a CEST spectrum (water signal as a function of saturation frequency) at each image pixel (29). MRI methods with fast temporal resolution, as demonstrated in these results, will facilitate MR CEST Spectroscopic Imaging studies.

The acquisition of multiple images before and after the injection of the PARACEST agent over the DCE MRI study provided several important advantages. Foremost, the pre-and postinjection images with selective saturation only at $\Delta\omega$ were compared to quantify PARACEST contrast. This obviated the need to acquire images with selective saturation at $-\Delta\omega$, which inherently doubled the temporal resolution and improved the CNR efficiency. For example, the temporal resolution of a single in vivo presat-RARE image with single average was 80 s/image, and the temporal resolution of a single in vivo presat-FLASH image with two averages was 76.8 s/image, which were half of the times required for comparable in vitro studies that required saturations at $\Delta\omega$ and $-\Delta\omega$. Selective saturation only at $\Delta\omega$ maintained steady-state saturation during presat-FLASH, which was critical for accurate quantification of PARACEST contrast with this method. This process of subtracting postcontrast images from precontrast images effectively cancels contrast mechanisms and other effects that are identical before and after the injection.

An analogous method for indirectly detecting PARACEST agents, termed “on-resonance” PARACEST MRI or OPARACHEE, has been demonstrated in vivo with a temporal resolution of 160–240 s (30). To the best of our knowledge, this study represents the first demonstrations of in vivo MRI signal changes that may be attributed to off-resonance PARACEST, which were greatly facilitated by using the PARACEST MRI methods with improved temporal resolutions. The long T_1 relaxation time of the tumor tissue allowed the use of the presat-RARE method, which generated a maximum 6.7% PARACEST effect. The relatively short T_1 relaxation time of liver tissue required the use of a presat-FLASH method, which generated a maximum 28.5% PARACEST effect (this high level was also facilitated by using liver-avid **Eu(2)**). More importantly, the CNR of the PARACEST contrast in the in vivo tumor and liver tissue studies reached the $2\sqrt{2}$ threshold for assigning the contrast to the presence of the PARACEST agent with 95% probability after 21 min and 14.08 min, respectively (Figs. 5D, 6D). To reach this CNR threshold at earlier time points, methods to increase image SNR are just as critical as methods to improve PARACEST contrast. For example, acquisition gating may remove cardiopulmonary motion artifacts from MR images of liver tissue, which would improve the CNR level without requiring the generation of a greater PARACEST effect. Other MRI pulse sequences with faster acquisition schemes or shorter saturation periods may be more applicable for particular biomedical applications than the specific RARE and FLASH methods used here. However,

the underlying principles used to establish these methods are still applicable to the design of more general PARACEST MRI methods for in vivo applications.

CONCLUSION

Two strategies have been developed that improve the temporal resolution of PARACEST MRI. In one case, a relatively long saturation is followed by a rapid readout. Under long T_1 relaxation conditions, this method shows only a minor loss in PARACEST detection and produces a temporal resolution as fast as 11.04 s per pair of images that are used to measure the PARACEST effect, or 5.52 s per image in a dynamic series of image acquisitions. Alternatively, one can use relatively short saturation periods with interleaved short acquisition periods. Under short T_1 relaxation conditions, this method shows a minor loss in PARACEST detection with a temporal resolution as fast as 25.6 s per pair of images, or 12.8 s per image in a dynamic series. Slower temporal resolutions may be used to increase the detected PARACEST effect by changing the RARE factor, TR, or number of averages. These methods with fast temporal resolutions enabled the in vivo detection of MRI signal changes that may be attributed to the PARACEST effect, although other dynamic effects may also contribute to these in vivo signal changes. MRI methods with fast temporal resolution may facilitate the evaluation of PARACEST and other dynamic effects, and the eventual translation of PARACEST MRI to clinical applications.

Acknowledgments

This research was supported by the Northeastern Ohio Animal Imaging Resource Center, an NIH funded program #R24CA110943, part of the Case Center for Imaging Research. Access to NMR spectrometers in the Department of Macromolecular Science and Engineering at Case Western Reserve University is also gratefully acknowledged.

Grant sponsor: NIH; Grant number: R24CA110943.

References

1. Ward KM, Aletras AH, Balaban RS. A new class of contrast agents for MRI based on proton chemical exchange dependent saturation transfer (CEST). J Magn Reson. 2000; 143:79–87. [PubMed: 10698648]
2. Guivel-Scharen V, Sinnwell T, Wolff SD, Balaban RS. Detection of proton chemical exchange between metabolites and water in biological tissues. J Magn Reson. 1998; 133:36–45. [PubMed: 9654466]
3. Aime S, Barge A, Delli Castelli D, Fedeli F, Mortillaro A, Nielsen FU, Terreno E. Paramagnetic lanthanide(III) complexes as pH-sensitive chemical exchange saturation transfer (CEST) contrast agents for MRI applications. Magn Reson Med. 2002; 47:639–648. [PubMed: 11948724]
4. McMahon MT, Gilad AA, Zhou J, Sun PZ, Bulte JW, van Zijl PC. Quantifying exchange rates in chemical exchange saturation transfer agents using the saturation time and saturation power dependencies of the magnetization transfer effect on the magnetic resonance imaging signal (QUEST and QUESP): Ph calibration for poly-L-lysine and a starburst dendrimer. Magn Reson Med. 2006; 55:836–847. [PubMed: 16506187]
5. Yoo B, Pagel MD. A PARACEST MRI contrast agent to detect enzyme activity. J Am Chem Soc. 2006; 128:14032–14033. [PubMed: 17061878]
6. Zhang S, Trokowski R, Sherry AD. A paramagnetic CEST agent for imaging glucose by MRI. J Am Chem Soc. 2003; 125:15288–15289. [PubMed: 14664562]

7. Aime S, Delli Castelli D, Terreno E. Supramolecular adducts between poly-L-arginine and [TmIIIdotp]: a route to sensitivity-enhanced magnetic resonance imaging-chemical exchange saturation transfer agents. Angew Chem Int Ed Engl. 2003; 42:4527–4529. [PubMed: 14520757]
8. Trokowski R, Ren J, Kalman FK, Sherry AD. Selective sensing of zinc ions with a PARACEST contrast agent. Angew Chem Int Ed Engl. 2005; 44:6920–6923. [PubMed: 16206314]
9. Aime S, Delli Castelli D, Terreno E. Novel pH-reporter MRI contrast agents. Angew Chem Int Ed Engl. 2002; 41:4334–4336. [PubMed: 12434381]
10. Zhang S, Malloy CR, Sherry AD. MRI Thermometry based on PARACEST agents. J Am Chem Soc. 2005; 127:17572–17573. [PubMed: 16351064]
11. Daldrup H, Shames DM, Wendland M, Okuhata Y, Link TM, Rosenau W, Lu Y, Brasch RC. Correlation of dynamic contrast-enhanced MR imaging with histologic tumor grade: comparison of macromolecular and small-molecular contrast media. AJR Am J Roentgenol. 1998; 171:941–949. [PubMed: 9762973]
12. Henderson E, Rutt BK, Lee TY. Temporal sampling requirements for the tracer kinetics modeling of breast disease. Magn Reson Imaging. 1998; 16:1057–1073. [PubMed: 9839990]
13. Tofts PS, Berkowitz B, Schnall MD. Quantitative analysis of dynamic Gd-DTPA enhancement in breast tumors using a permeability model. Magn Reson Med. 1995; 33:564–568. [PubMed: 7776889]
14. Shames DM, Kuwatsuru R, Vexler V, Muhler A, Brasch RC. Measurement of capillary permeability to macromolecules by dynamic magnetic resonance imaging: a quantitative noninvasive technique. Magn Reson Med. 1993; 29:616–622. [PubMed: 8505897]
15. Zhang S, Merritt M, Woessner DE, Lenkinski RE, Sherry AD. PARACEST agents: modulating MRI contrast via water proton exchange. Acc Chem Res. 2003; 36:783–790. [PubMed: 14567712]
16. Woessner DE, Zhang S, Merritt ME, Sherry AD. Numerical solution of the Bloch equations provides insights into the optimum design of PARACEST agents for MRI. Magn Reson Med. 2005; 53:790–799. [PubMed: 15799055]
17. Forsen S, Hoffman RA. Study of moderately rapid chemical exchange reactions by means of nuclear magnetic double resonance. J Chem Phys. 1963; 2892
18. Woessner DE. Nuclear transfer effects in nuclear magnetic resonance (NMR) pulse experiments. J Chem Phys. 1961; 35:41–48.
19. Zhang S, Sherry AD. Physical characteristics of lanthanide complexes that act as magnetization transfer (MT) contrast agents. J Solid State Chem. 2003; 171:38–43.
20. Zhang S, Winter P, Wu K, Sherry AD. A novel europium(III)-based MRI contrast agent. J Am Chem Soc. 2001; 123:1517–1518. [PubMed: 11456734]
21. Ali MM, Woods M, Suh E, Kovacs Z, Tircso G, Kodibagkar V, Sherry AD. Albumin-binding PARACEST agents. J Biol Inorg Chem. 2007; 12:855–865. [PubMed: 17534672]
22. Hennig J, Nauerth A, Friedburg H. RARE imaging: a fast imaging method for clinical MR. Magn Reson Med. 1986; 3:823–833. [PubMed: 3821461]
23. Hennig J, Friedburg H. Clinical applications and methodological developments of the RARE technique. Magn Reson Imaging. 1988; 6:391–395. [PubMed: 3185132]
24. Haase A, Frahm J, Matthaei D, Haenicke W, Merboldt KD. FLASH imaging, rapid NMR imaging using low flip-angle pulses. J Magn Reson. 1986; 67:258–266.
25. Haacke, EM.; Brown, RW.; Thompson, MR.; Venkateson, R. Magnetic resonance imaging: physical principles and sequence design. New York: Wiley-Liss; 1999. p. 349
26. Abramoff MD, Magelhaes PJ, Ram SJ. Image processing with ImageJ. Biophotonics Int. 2004; 11:36–42.
27. Aime S, Castelli DD, Terreno E. Highly sensitive MRI chemical exchange saturation transfer agents using liposomes. Angew Chem Int Ed. 2005; 44:5513–5515.
28. Oshio K, Singh M. Correction of T2 distortion in multi-excitation RAREsequence. Medical Imaging, IEEE Transactions on. 1992; 11:123–128.
29. Gillen, J.; Mina, K.; van Zijl, P.; Zhou, J. WAter Saturation Shift Referencing (WASSR) for chemical exchange saturation transfer experiments. Proceedings of the 17th Annual Meeting of ISMRM; Toronto, Canada. 2008. abstract 1423

30. Vinogradov E, He H, Lubag A, Balschi JA, Sherry AD, Lenkinski RE. MRI detection of paramagnetic chemical exchange effects in mice kidneys in vivo. Magn Reson Med. 2007; 58:650–655. [PubMed: 17899603]

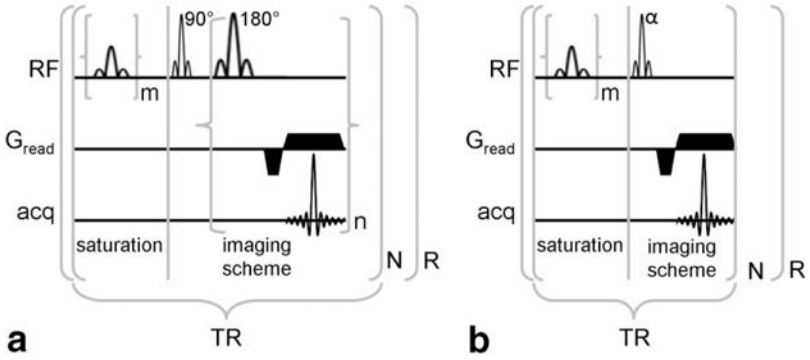

FIG. 1.

A: Pulse sequence diagram of a PARACEST detection method with a multiple-echo imaging scheme. **B:** Pulse sequence diagram of a PARACEST detection method with a short repetitive saturation scheme. For both schemes, m represents the number of selective saturation pulses that comprise τ_s, and R represents the number of repetitions. For presat-RARE, n represents the number of echos that are acquired per excitation (a.k.a., RARE factor), the product of n and N represents the number of phase encoding steps, and the first lobe of G_{read} alternates in phase for each successive echo. For presat-FLASH, N represents the number of phase encoding steps.

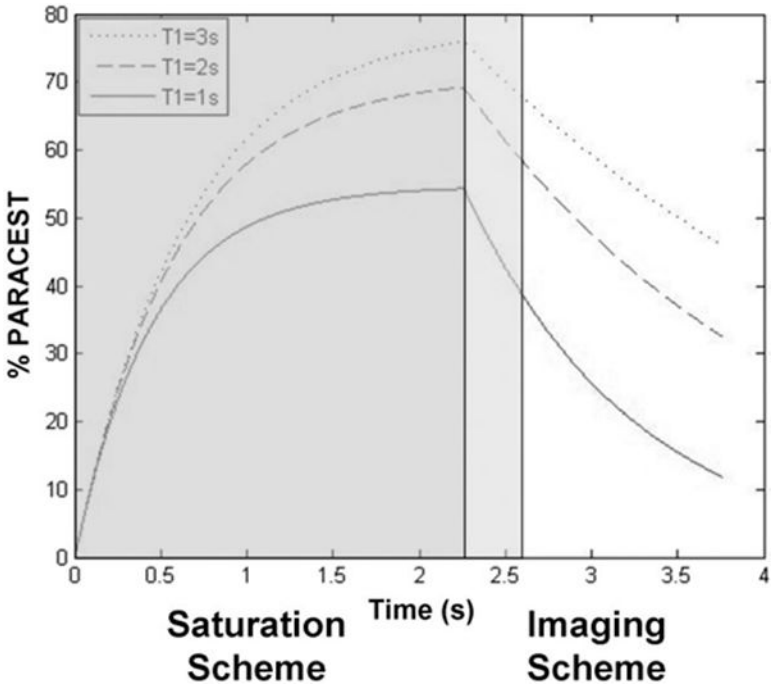

FIG. 2.

Simulations of the water signal during the saturation scheme and after the removal of saturation pulses, using Equations [6] and [7]. The parameters are τ_s = Time (for Time < 2.25 s), TE^{eff} = 0 (for Time < 2.25 s), TE^{eff} = Time – 2.25 s (for Time ≥ 2.25 s), τ_w = 300 μs, T_{1w} = 1 s, 2 s, and 3 s.

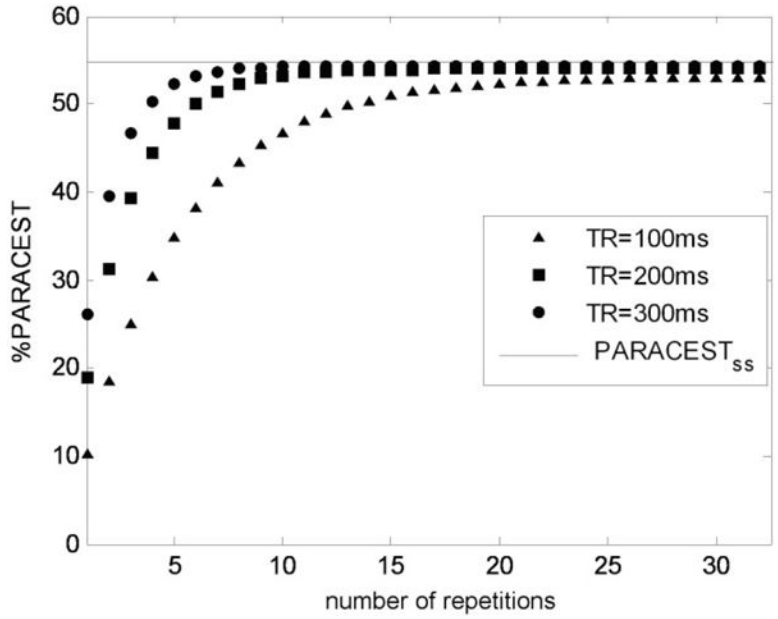

FIG. 3.

Simulation of a build-up and maintenance of PARACEST by using short repetitive saturation pulses. The parameters are τ_s = TR – TE^{eff}, TE^{eff} = 7.678 ms, τ_w = 300 μs, T_{1w} = 1 s. $PARACEST_{SS}$ is the theoretically calculated steady state PARACEST effect. Note that only the first 1–32 acquisitions of 128 phase encoding steps are displayed to show the steady state build-up.

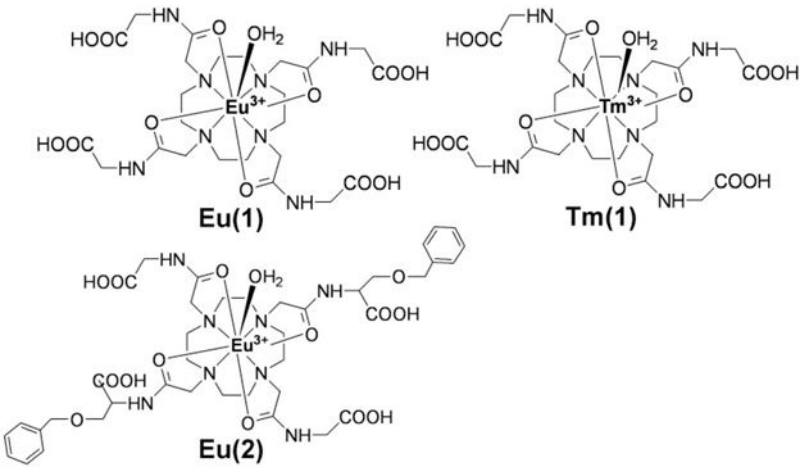

FIG. 4.

Structures of Eu(III)DOTAM-Gly (**Eu(1)**), Tm(III)DOTAM-Gly (**Tm(1)**) and Eu(III)DOTA-OBS2Gly2COOH (**Eu(2)**).

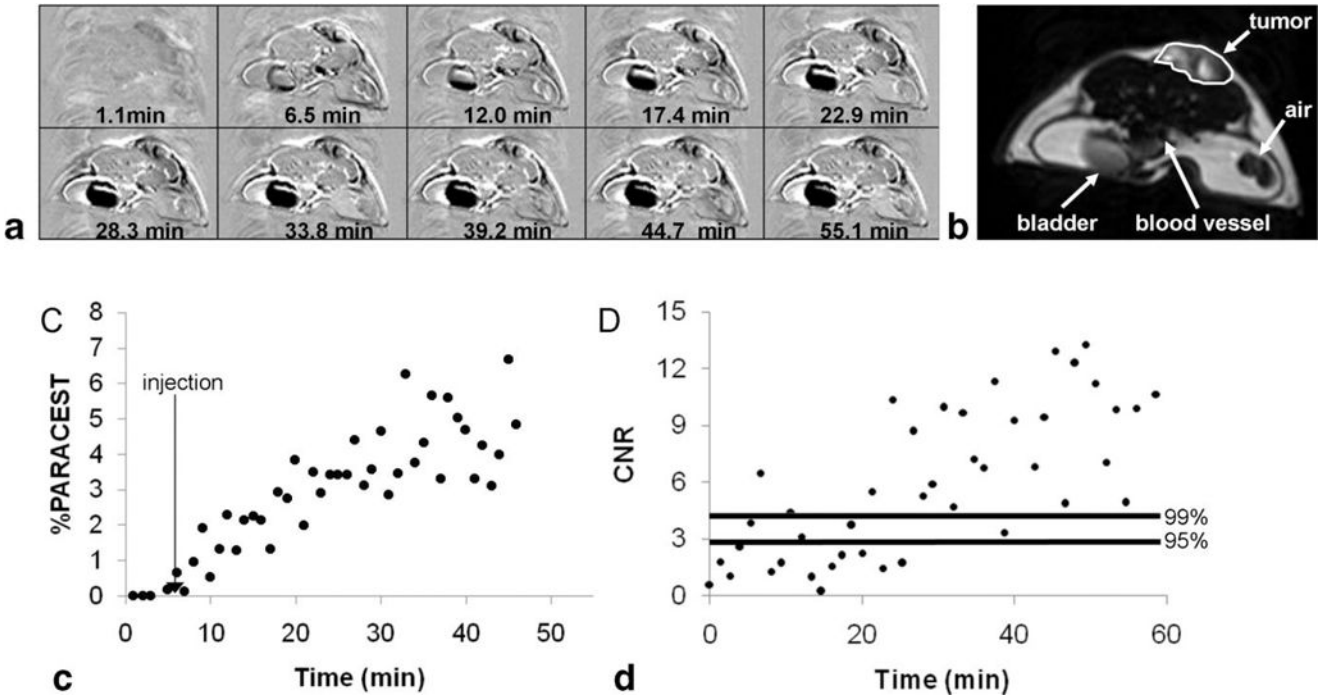

FIG. 5.

The in vivo DCE MRI study of tumor tissue with a presat-RARE MRI method with a RARE factor of 16 (80 s/image). The contrast agent was **Tm(1). A:** The parametric maps represent the difference between postinjection images and the average of the preinjection images at different time points. **B:** A representative image with marked tumor ROI area for quantitative analysis. **C:** The dynamic change in PARCEST contrast of tumor ROI. **D:** The corresponding CNR of the PARACEST contrast for the same ROI. Horizontal lines represent the 95% and 99% probability levels that the CNR was generated from the PARACEST agent.

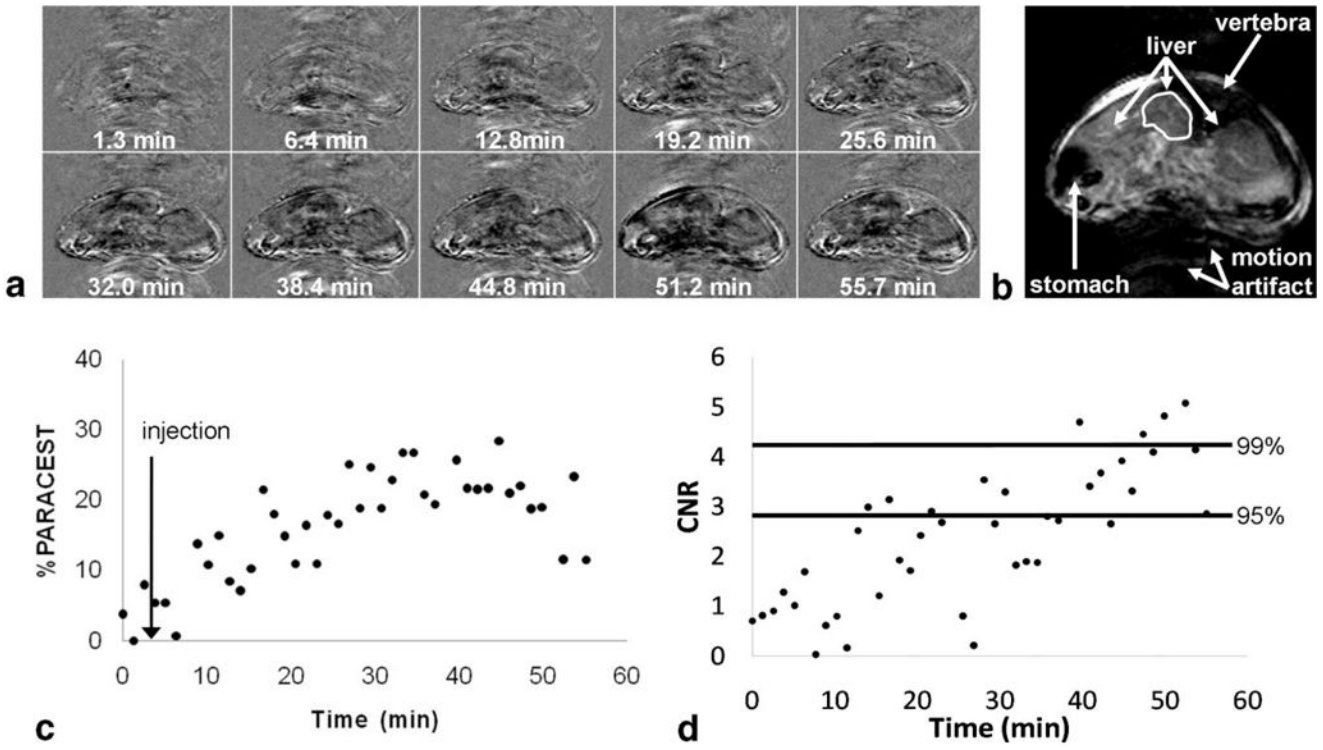

FIG. 6.

The in vivo DCE MRI study of liver with a presat-FLASH MRI method with a 300 ms TR (76.8 s/image). The contrast agent was **Eu(2). A:** The parametric maps represent the difference between post-injection images and the average of the preinjection images at different time points. **B:** A representative image with marked ROI area for quantitative analysis. **C:** The dynamic change in PARCEST contrast of liver ROI. **D:** The corresponding CNR of the PARACEST contrast for the same ROI. Horizontal lines represent the 95% and 99% probability levels that the CNR was generated from the PARACEST agent.

Table 1

Simulated PARACEST Effects of 20 mM **Eu(1)** With Different PARACEST MRI Methods That Employ a Long τ_S

	% PARACEST						
	presat-GRE	presat-RARE			Ratio of presat-RARE/presat-GRE		
	τ_S = 10 s TE^{eff} = 0 s	τ_S = 3.4 s TE^{eff} = 0s	τ_S = 2.26 s TE^{eff} = 0s	τ_S = 2.26 s TE^{eff} = 0.32 s	τ_S = 3.4 s TE^{eff} = 0 s	τ_S = 2.26 s TE^{eff} = 0 s	τ_S = 2.26 s TE^{eff} = 0.32 s
T_{1W} = 1s	54.8%	54.8%	54.4%	39.6%	99.9%	99.3%	72.2%
T_{1W} = 2s	70.8%	70.6%	69.3%	59.1%	99.7%	97.9%	83.5%
T_{1W} = 3s	78.4%	78.0%	76.1%	68.4%	99.5%	97.1%	87.2%

Table 2

Simulated PARACEST Effects of 20 mM **Eu(1)** With Different PARACEST MRI Methods That Employ a Short τ_S

	% PARACEST						
	presat-GRE	presat-FLASH			Ratio of presat-FLASH/presat-GRE		
	τ_S = 10 s TE^{eff} = 0 s	τ_S = 292 ms TR = 300 ms	τ_S = 193 ms TR = 200 ms	τ_S = 93 ms TR = 100 ms	τ_S = 292 ms TR = 300 ms	τ_S = 193 ms TR = 200 ms	τ_S = 93 ms TR = 100 ms
T_{1W} = 1s	54.8%	54.3%	54.0%	53.1%	99.1%	98.5%	96.9%
T_{1W} = 2s	70.8%	70.3%	70.1%	69.3%	99.3%	99.0%	97.1%
T_{1W} = 3s	78.4%	78.1%	77.8%	77.2%	99.6%	99.3%	98.5%

Table 3

Quantitative Comparison of MRI Methods That Detect the PARACEST Effect of a 20 mM Phantoms of **Eu(1)** and **Tm(1)**

Methods	Time (s)	Eu(1)				Tm(1)			
		% CEST	% CEST relative to presat-GRE	CNR[a]	CNR Efficiency ($s^{-1/2}$)[b]	% CEST	% CEST relative to presat-GRE	CNR[a]	CNR Efficiency ($s^{-1/2}$)[b]
Presat-GRE	580.4	36.23	100	41.43	1.72	9.78	100	8.52	0.35
Presat-RARE rare factor = 1	589.4	35.63	98.34	26.84	1.11	9.60	98.13	5.47	0.23
Presat-RARE rare factor = 4	147.3	35.36	97.59	20.53	1.69	9.24	94.49	2.28	0.19
Presat-RARE rare factor = 8	74.6	35.11	96.91	15.16	1.75	8.88	90.77	1.28	0.15
Presat-RARE rare factor = 16	38.3	34.48	95.17	11.12	1.80	8.57	87.62	0.48	0.08
Presat-RARE rare factor = 32	20.1	33.85	93.43	6.67	1.49	7.64	78.06	0.12	0.03
Presat-RARE rare factor = 64	11.0	32.80	90.53	3.36	1.01	6.06	61.95	0.04	0.01
Presat-FLASH T_R = 300ms	76.8	28.54	78.78	1.61	0.18	8.72	89.17	2.99	0.34
Presat-FLASH T_R = 200ms	51.2	27.85	76.85	1.07	0.15	8.00	81.78	1.90	0.27
Presat-FLASH T_R = 100ms	25.6	26.61	73.43	0.52	0.10	6.99	71.48	0.64	0.13

[a] $CNR = (M_0 - M_S)/[\sqrt{2}\ (noise)]$.

[b] CNR Efficiency = CNR/√time.